XAFS

A Technique to Probe Local Structure

Steven D. Conradson as told to Jay Schecker

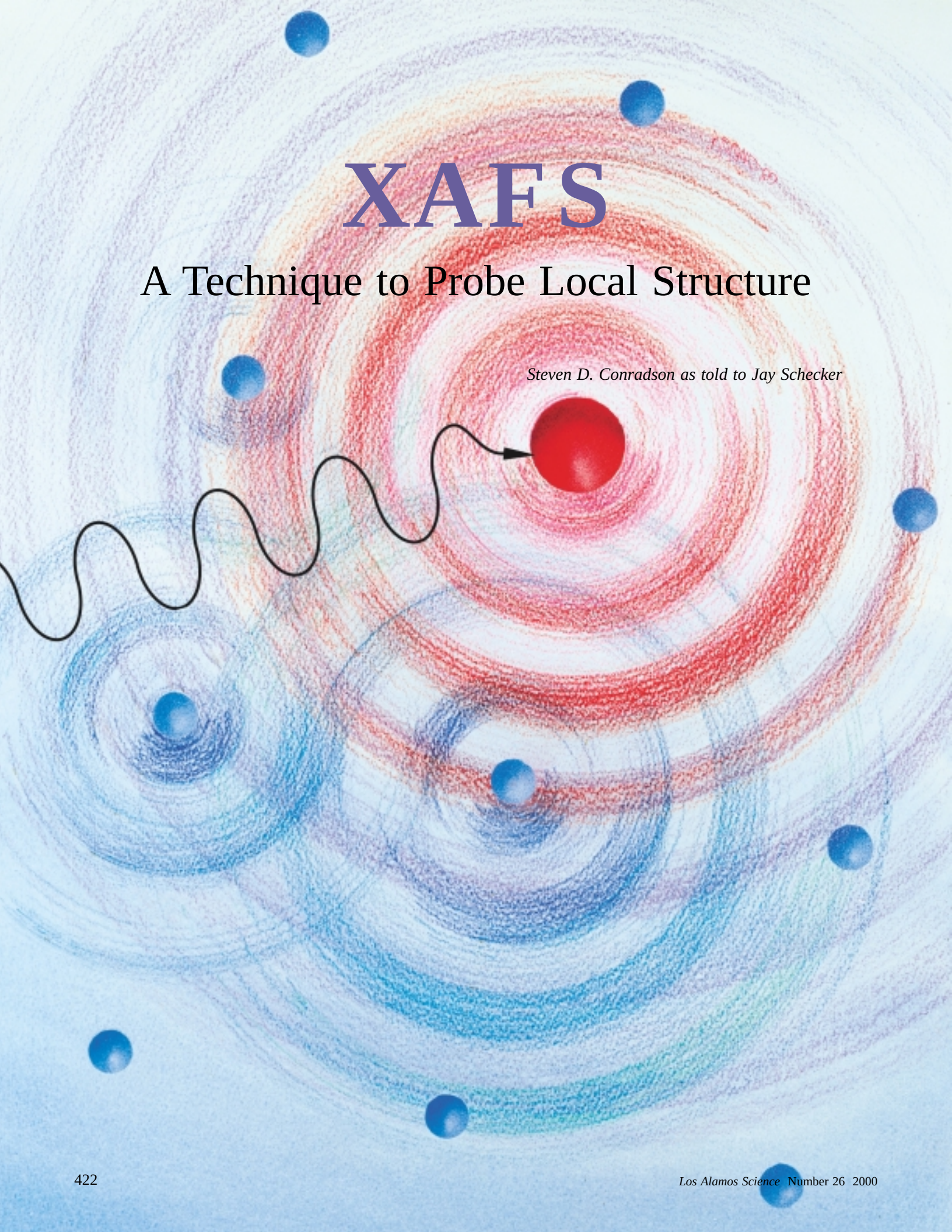

From the instant of their creation inside a nuclear fuel rod and forever thereafter, plutonium atoms are found in association with other atoms. In a solid, for example, plutonium becomes part of the lattice or matrix that makes up the condensed matter, while in solution, the element typically forms large molecular complexes in which many ligands bond to the central plutonium ion. To a large degree, the number, type, and arrangement of atoms or molecules that surround a plutonium atom determine its behavior. Thus if we are to understand and control plutonium's behavior in chemical processes, in the natural environment, or in stockpiled nuclear weapons, we need insight into the "local" structure of the atoms that surround it.

X-ray absorption fine structure (XAFS) spectroscopy is one of the most powerful tools we have for mapping local structure. In this technique, we probe a sample with x-rays that are tuned to the energy of a core electron shell in the element we wish to study. We monitor how many x-rays are absorbed as a function of their energy. If taken with sufficient accuracy, the spectrum exhibits small oscillations that are the result of the local environment's influence on the target element's basic absorption probability. From the spectrum, we can extract the distances between the absorber and its near-neighbor atoms, the number and type of those atoms, and the oxidation state of the absorbing element—all parameters that determine local structure. By selecting a different x-ray energy, we can obtain this information for any element in the sample.

A fundamental aspect of XAFS spectroscopy is that it is a "short-range" technique—the target element does not have to be part of a large, coherent domain of atoms. In fact, the sample need not have a periodic structure. XAFS spectroscopy is one of the few techniques that can probe the molecular structure of chemical species in solution or in amorphous solids such as a glass. For crystalline solids, XAFS provides information that is complementary to long-range techniques such as x-ray diffraction, which derives its signal by summing the contributions of millions of atoms arrayed over hundreds or thousands of angstroms. Whereas x-ray diffraction provides a picture of the average structure of coherent portions of the solid, XAFS yields insight into the average structure surrounding each absorption site.

XAFS spectroscopy began to emerge as a practical experimental tool in the early 1970s, after Dale Sayer, Edward Stern, and Farrel Lytle demonstrated that a Fourier transform could be used to analyze the absorption spectra. Their work coincided with the development of synchrotron x-ray sources that emit enough x-ray photons in the right spectral range to enable rapid, highly accurate absorption measurements. With the subsequent availability of inexpensive computing power to analyze the data and implement the increasingly accurate theoretical models, XAFS flourished.

Only a few isolated XAFS studies, however, were done on the transuranics (elements with atomic numbers greater than that of uranium). In 1993, Los Alamos National Laboratory established the first systematic XAFS program for studying the transuranics and other highly radioactive samples. One of our goals for the first set of experiments was to determine the structure of plutonium complexes in concentrated nitric acid solution. That information was needed to improve our nitric acid recovery process for plutonium (see the article "Molecularly Engineered Resins for Plutonium Recovery" on page 454). Our program involved developing the containment technology and safety procedures that would allow us to mount hazardous samples at the Stanford Positron-Electron Asymmetric Ring (SPEAR) synchrotron at Stanford University. It also involved assembling the teams of dedicated people who would carry out the work.

We have since used XAFS spectroscopy to study the local structure of plutonium alloys and to deduce the structure of hundreds of plutonium complexes in solutions, solids, slurries, soils, and sludges. In collaboration with scientists from many different institutions, we have also examined thorium, uranium, neptunium, americium, and curium complexes as part of our general program to advance the molecular science of the actinides. In this article,[1] we will delve into the theory and practice of XAFS and describe a few applications of the technique in probing uranium speciation and the structure of plutonium colloids. Other applications are discussed within several articles in this volume of *Los Alamos Science* (for example, see "Characterizing the Plutonium Aquo Ions by XAFS Spectroscopy" on page 418.)

[1]Portions of this article were adapted from a 1998 article by S. D. Conradson, "Applications of XAFS to Materials and Environmental Science" (*Applied Spectroscopy* **52**: 252A), with permission from the publisher, the Society for Applied Spectroscopy.

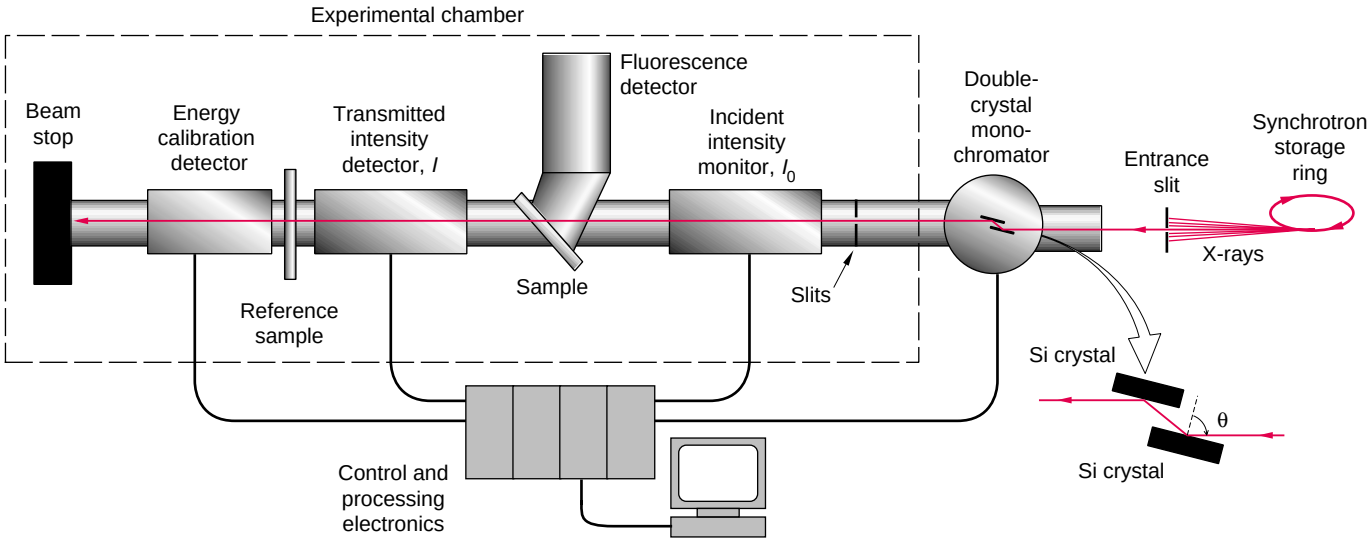

Figure 1. Typical Experimental Setup for XAFS

The full spectrum of x-rays emitted from a synchrotron pass through an entrance slit (which helps collimate the x-rays) before entering a double-crystal monochromator. The x-rays diffract off the crystals' lattice planes, which are aligned at an angle θ with respect to the incoming beam. Because of the Bragg scattering condition $n\lambda_i = 2d\sin\theta$, only x-rays of energy $E_n = nhc/\lambda_i$ can reflect off the crystals. Any of several techniques can eliminate the higher harmonics, so that only the fundamental (n = 1) makes it through the exit slits. Different x-ray energies can be selected by changing the angle θ of the crystals. The monochromatic beam passes through an ion chamber that monitors the beam intensity I_0 by absorbing part of it. The beam then passes through the sample, and the intensity of the transmitted x-ray I is measured by a second ion chamber. Taking the log of the ratio of I/I_0 yields the absorption. We can also determine the sample's absorption by measuring the intensity of its x-ray fluorescence with a detector that is out of the beam path. Finally, the beam passes through a reference sample whose absorption edge is used to help correct for uncertainties in the beam's energy.

XAFS Spectroscopy

Figure 1 shows a schematic diagram of a typical XAFS experiment. The broadband x-ray spectrum from a synchrotron is directed into a double-crystal monochromator. This instrument houses two parallel silicon crystals that are aligned at an angle θ with respect to the incoming beam. Only specific x-ray wavelengths (a fundamental plus its harmonics) can satisfy the Bragg scattering condition for constructive interference from the crystals' lattice planes and therefore be passed. After the higher harmonics are rejected, a "single" x-ray wavelength emerges from the instrument: because the relative bandwidth of the emerging beam is about 10^{-4}, that is, 10-kilo-electron-volt (keV) x-rays emerge with an energy spread of only 1 eV, the beam is deemed monochromatic. By changing the orientation of the two crystals, we can select different energies; thus the monochromator allows us to probe a sample with a set of monochromatic x-rays that span a wide energy range.

The intensity I_0 of the x-ray beam is monitored with a detector (usually a gas ionization chamber) before the beam impinges on a sample. For an ideal sample, between 50 and 90 percent of the x-ray beam intensity is absorbed, while the remainder of the beam passes through. In a transmission-mode experiment, a second detector placed behind the sample monitors the intensity I of the transmitted beam. The latter will follow Beer's Law:

$$I = I_0 e^{-\mu(E)L} \quad , \qquad (1)$$

where $\mu(E)$ is the energy-dependent absorption coefficient of the sample, L is the sample thickness, and E is the energy of the incident x-ray.

In general, $\mu(E)$ decreases approximately as E^{-3} with increasing x-ray energy. At certain energies, however, it abruptly jumps to a higher value, as indicated in Figure 2. These "jumps" in the absorption profile are called absorption edges. They occur whenever E equals the binding energy of an electron in one of the elements in the sample, and thus the energies at which edges appear are unique for each element. During an experiment, the x-rays are scanned with high accuracy over an absorption edge of the target element, and by comparing I with I_0, we measure $\mu(E)$ versus E for that element.

During the absorption process, an electron moves from its initial bound state to a final unbound state that lies

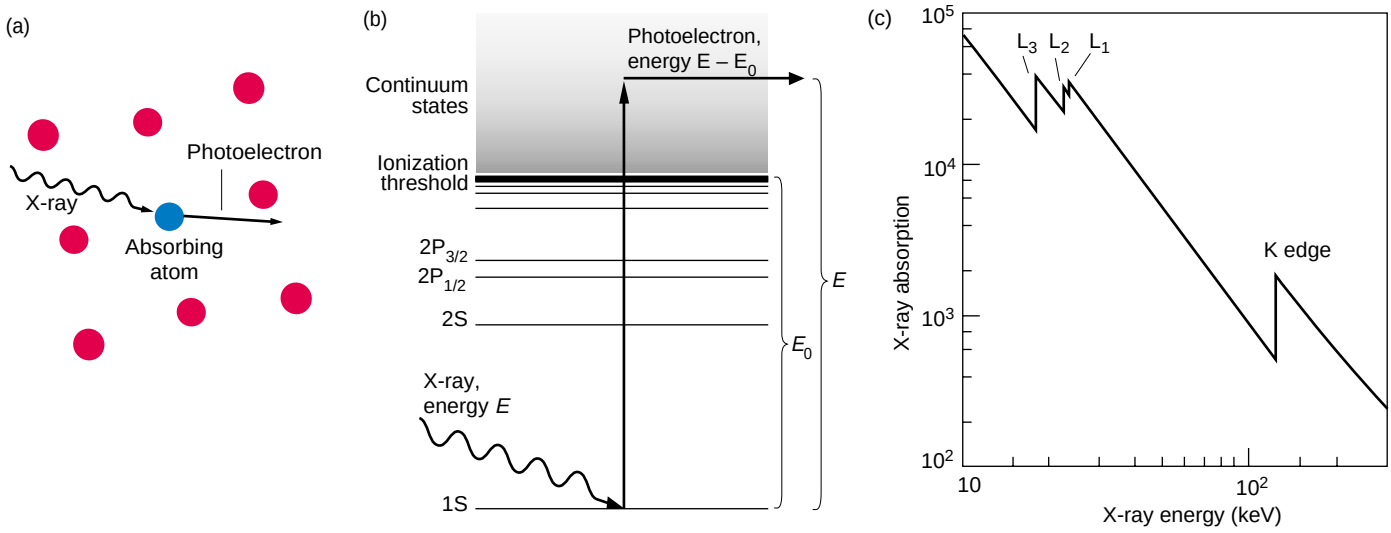

Figure 2. X-Ray Absorption

(a) An absorbing atom (blue) is shown here surrounded by several other atoms (red). Whenever the energy of an x-ray is greater than the binding energy of one of the absorbing atom's core electrons, the electron is liberated. (b) This schematic energy-level diagram of an absorbing atom shows the atom's first few core-electron orbitals: 1S, 2S, $2P_{1/2}$, and $2P_{3/2}$. The ionization potential energy is denoted by E_0. With the absorption of a photon of energy E, the electron undergoes a transition to an unbound state in the continuum and, by conservation of energy, acquires a kinetic energy ($E - E_0$). (c) The abrupt jumps in this simplified absorption spectrum are the absorption edges, which correspond to the excitation of an electron from a specific orbital. The absorption edge due to excitation of the 1S electron is called the K edge, while excitations from the less strongly bound 2S, $2P_{1/2}$, and $2P_{3/2}$ electrons are called the L_1, L_2, and L_3 edges, respectively.

above the ionization potential E_0 of the atom. (This electron is often referred to as a photoelectron since it is liberated in a photoabsorption process.) If we assume that a single electron absorbs all of the photon energy, then by conservation of energy, the photoelectron is kicked free with a kinetic energy ($E - E_0$).

At the x-ray energies available from today's synchrotrons—extending past 10 keV—the electron is ejected from one of the low-lying orbitals of the atom (the 1S, 2S, $2P_{1/2}$, or $2P_{3/2}$ orbitals). The absorption edge due to excitation of the 1S electron is called the K edge, while excitations from the less strongly bound 2S, $2P_{1/2}$, and $2P_{3/2}$ electrons are called the L_1, L_2, and L_3 edges, respectively.

The K-edge energies of plutonium and the other actinides are well above 100 keV, which is difficult to access experimentally. Also, K-shell electrons have a lower absorption cross section than L-shell electrons. Thus our XAFS studies of the actinides are typically done on the L_2 and L_3 edges. The energy of the L_3 edge of plutonium varies between 18.056 and 18.061 keV, depending on the oxidation state of the plutonium ion.

Figure 3 shows the L_3 edge of platinum, obtained from a thin platinum foil. The spectrum has numerous small oscillations on the high-energy side of the edge. As explained in the next section, those oscillations result because the local atomic environment affects the probability that the target atom absorbs the x-ray photon. The effect is small: just 500 eV from the edge, the difference between the absorption coefficient μ of an element in the sample and the absorption coefficient μ_0 of the free atom may be only a few tenths of a percent. While it is difficult to measure such small changes, the synchrotron's stable high flux of photons allows us to do so with accuracy and precision.

The oscillations that start about 30 eV beyond the peak of the absorption edge and that persist for another 1000 eV are known as the extended x-ray absorption fine structure (EXAFS). In this region, the kinetic energy of the photoelectron is large compared with its interaction energy with nearby atoms, which is on the order of 3 eV. The local environment, therefore, only slightly perturbs the final state of most of the photoelectrons, and we can use perturbation theory to construct a theory of the physics underlying the EXAFS. Such work began in the 1930s, and a fairly complete theory was in place by the early 1960s. The EXAFS encodes most of the local structure parameters, such as the distance R to nearby atoms and both the number N and atomic number Z of those atoms.

The narrow region that starts slightly before the absorption edge and extends about 30 eV beyond the peak also shows structure—the x-ray absorption near-edge structure (XANES). In this region, the photoelectron has less kinetic energy, and its interactions with the

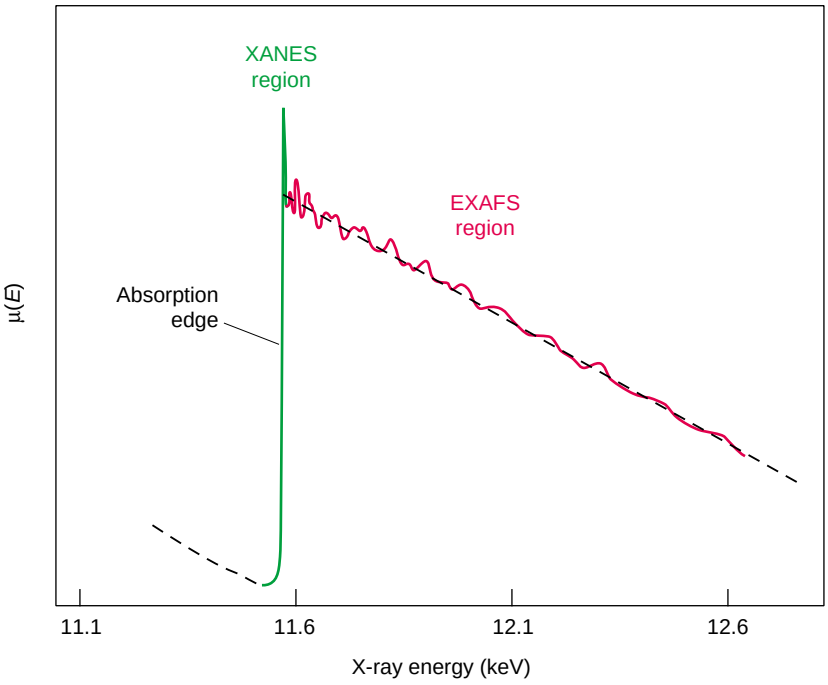

Figure 3. Typical XAFS Spectrum
In this XAFS spectrum of a platinum foil, small oscillations modify the basic absorption coefficient of the free atom μ_0 (represented by the dashed line). The small peaks and shoulders that modify the absorption edge and extend about 30 eV beyond it are known as the x-ray absorption near-edge structure (XANES). The XANES region contains information about the ionization potential and oxidation state of a chemical species and often exhibits features that are characteristic of specific molecular structures. The oscillations that begin approximately 30 eV beyond the absorption edge are called the extended x-ray absorption fine structure (EXAFS). The EXAFS region encodes structural information, such as the distance, type, and number of neighboring atoms.

local environment are more difficult to interpret. However, researchers have long realized that the oxidation state of the absorbing atom can be extracted from the XANES spectrum. (More information about this region is given in the XANES box on page 432.)

Originally, the XANES and EXAFS regions were thought to reflect different physical processes. But increasingly accurate calculations have indicated that with few exceptions, all of the peaks and valleys in the XANES spectra, including the maximum of the absorption edge, can be explained by the same physics that leads to the EXAFS. Today, both regions are jointly referred to as the XAFS. Because it is easier to describe, we will focus on the EXAFS in the discussion that follows.

EXAFS Theory

The extended fine structure fundamentally derives from the wave nature of photoelectrons. When an electron is ejected from an isolated atom, the photoelectron's final state can be represented by an expanding spherical wave. But when the absorbing atom is not isolated, the photoelectron can scatter from the nearby atoms. At the "large" kinetic energies in the EXAFS region, it is reasonable to assume that the photoelectron scatters only once as it leaves (single-scattering approximation). The final electron state is then a superposition of the outgoing and scattered waves.

Interference between those two wave components affects the probability $P(E)$ that the target atom absorbs the incoming x-ray photon. To see this, recall that in quantum mechanics the absorption probability is proportional to the square of the transition matrix element that connects the initial and final states of the electron:

$$P(E) \sim |\langle \psi_f \mid H_{int} \mid \psi_i \rangle|^2 \quad , \qquad (2)$$

where ψ_i and ψ_f are the initial- and final-state wave functions, respectively, and H_{int} is the part of the Hamiltonian that describes the interaction between the electron and the x-ray radiation field. The matrix element is evaluated over all space, but its value is nonzero only where the initial- and final-state wave functions overlap. Since the initial state ψ_i is one of the low-lying core orbitals and is highly localized, the matrix element (which involves integrating ψ_i and the complex conjugate of ψ_f over space) depends only on the part of the final-state wave function that exists near the center of absorber. Only those portions of the outgoing wave that scatter back to the absorber (backscatter) affect the probability of x-ray absorption.

If (in the particle picture) the photoelectron elastically scatters from a nearby atom, then (in the wave picture) the backscattered wave will remain coherent with the outgoing wave. As seen in Figure 4, the two waves will interfere at the absorbing atom, either increasing or decreasing the amplitude of the final-state wave function. The amount of interference naturally depends on the amplitude and phase of the backscattered wave. The phase in turn depends on the distance between the absorbing and scattering atoms and on the photoelectron wavelength λ. This wavelength is related to the photoelectron momentum p through the de Broglie relation,

$$\lambda = \frac{h}{p} \quad , \qquad (3)$$

where h is Planck's constant. The momentum is a function of the

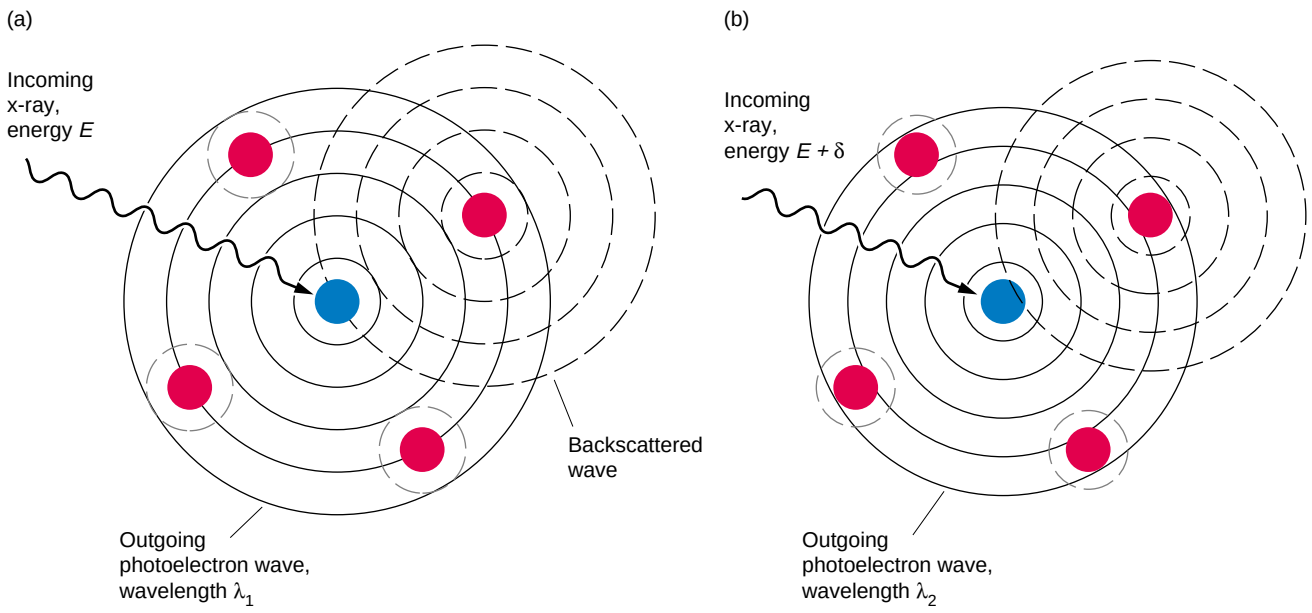

Figure 4. Interference in the Final-State Wave Function

The wave function of a photoelectron liberated from an absorbing atom (blue) is described by an outward-propagating spherical wave. This wave can backscatter from a nearby atom (red) and interfere with itself back at the absorber. (a) In constructive interference, wave crests (solid and dashed lines) meet in the center of the absorbing atom and increase the amplitude of the final-state wave function. Maximum constructive interference is shown here. (b) When an x-ray of a different energy is absorbed, the photoelectron wavelength and the interference change. Shown here is maximum destructive interference, when the waves are 180 degrees out of phase at the atom. The amplitude is decreased. Over a range of energies, the final-state wave function will increase or decrease many times, resulting in energy-dependent oscillations in the atom's absorption probability.

electron's kinetic energy,

$$p = \sqrt{2m\left(E - E_0\right)} \quad , \tag{4}$$

where m is the electron mass, and thus the wavelength of the photoelectron depends on its kinetic energy:

$$\lambda = \frac{h}{\sqrt{2m\left(E - E_0\right)}} \quad . \tag{5}$$

As the x-ray energy E increases, the photoelectron wavelength λ decreases. The relative phase between the outgoing and backscattered waves changes and alters the amplitude of the final-state wave function . Hence, the atom's photoabsorption cross section becomes modified as a function of x-ray energy.

Because the amplitude of the backscattered wave will vary depending on the position R of the backscattering atom (as R^{-2}) and on the type of atom (since the scattering function depends on the atomic number Z of the scatterer), every atom in the local environment will uniquely modify the free-atom absorption. But crystal lattices and molecules are often highly symmetric; a number of identical atoms will typically surround the target atom at a common radius. These atoms are said to occupy a spherical shell of radius R. In a complex molecule or solid-state structure, numerous shells will be nested around the target atom, and we can construct a model in which the photoelectron scatters not from individual atoms, but from individual shells (see Figure 5).

Standard EXAFS Equation. In deriving a model for the EXAFS, we assume that the local environment perturbs the absorption coefficient μ_0 of the free atom. The measured absorption coefficient is μ:

$$\mu = \mu_0 \left[1 + \chi(k)\right] \quad , \tag{6}$$

where $\chi(k)$ describes the EXAFS, and $k = 2\pi/\lambda$ and is the magnitude of the photoelectron wave vector. By incorporating the assumptions discussed above (that is, photoelectron kinetic energies of ~30 eV or higher and only single scattering,[2] we can derive the standard expression for EXAFS:

$$\chi(k) = \sum_j A_j(k)\ e^{-\beta_j(k)} \times \sin\left(2kR_j + \Phi_j(k)\right) \quad . \tag{7}$$

This equation is a sum over expo-

[2]Other assumptions include neglecting the x-ray's polarization and assuming only dipole interactions between the absorber and the radiation field.

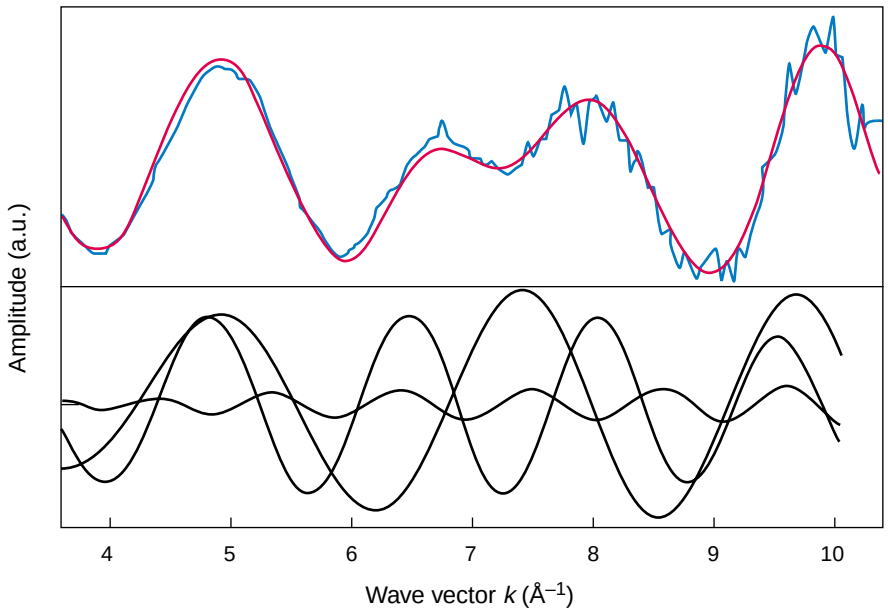

Figure 5. An EXAFS Spectrum

The local structure surrounding a target atom can be modeled as a series of spherical shells, where each shell has a unique radius and contains a finite number of identical atoms. A photoelectron that backscatters from a particular shell acquires a unique energy-dependent phase and amplitude, so its contribution to the EXAFS can be discerned. The upper graph shows part of a measured EXAFS spectrum (blue line) and its theoretical fit (red line). The lower graph shows the three waves that compose the fit. Each wave corresponds to backscattering from a different shell. The waves are plotted as a function of wave vector $k = 2\pi/\lambda$.

nentially damped sine waves, where each wave accounts for the backscattering of an electron from a shell of atoms (the index j references a shell).

The term $2kR_j$ in the argument of the sine function results from the phase shift of the photoelectron as it leaves the absorbing atom, backscatters from an atom at position R_j, and returns. The additional phase shift $\Phi_j(k)$ arises because the photoelectron travels through the spatially varying potentials of the absorbing and backscattering atoms.

The amplitude $A_j(k)$ of each wave is given by

$$A_j(k) = \frac{N_j}{kR_j^2} f_j(k)\ S_0^2 \quad , \qquad (8)$$

where N_j is the number of atoms in each shell and $f_j(k)$ is the magnitude of the complex function describing the scattering. The last term, S_0^2, is a loss term that accounts for multielectron excitations and inelastic scattering.

We see that the amplitude of each wave is a function of the parameters N_j and R_j. In addition $f_j(k)$, as well as the phase shift $\Phi_j(k)$, is a function of the atomic number Z_j. Thus, we can extract those three primary pieces of information for each shell in the EXAFS data. But the amplitude decreases as R_j^{-2}, so the contributions from more-distant scattering shells decrease rapidly. The EXAFS is often not useful for obtaining information from shells that are more than 4 or 5 angstroms from the target.

The exponential damping term in Equation (7) accounts for additional processes that modify the final-state wave function. This term is also a product:

$$e^{-\beta_j(k)} = e^{\frac{-2R_j}{\lambda_e}}\ e^{-2k^2\sigma_j^2} \quad . \qquad (9)$$

The first exponential takes into account the finite lifetime of the final state. The photoelectron leaves behind a hole in the absorbing atom's core configuration, and filling the hole with a new electron represents the end of the final state. The hole lifetime is typically about 1 femtosecond. The photoelectron also has a "lifetime," since it can scatter out of the system. Both processes can destroy the coherence between the components of the final-state wave function and hence wipe out the interference. The form of this damping term is phenomenological; it is parameterized in terms of the mean free path λ_e of the photoelectron.

The second exponential accounts for the fact that atoms are in constant thermal motion; hence the positions of the atoms within a shell are distributed about an average radius R_j. Photoelectrons scatter from each atom with a slightly different phase, with a subsequent "smearing" of the EXAFS. Localized strains (static disorder) will similarly affect atomic positions. By assuming that the positions vary according to a Gaussian distribution, we can derive the exponential form of the correction term, where the parameter σ_j acts like a pairwise Debye-Waller factor between the absorber and a scattering atom. Both thermal and static disorders are modeled by the second exponential.

In 1971, Stern, Sayers, and Lytle showed that Equation (7) could be analyzed by a Fourier transform. The EXAFS, $\chi(k)$, which is parameterized in terms of the wave vector k, could be transformed into a radial structure function $\chi(R)$ that represents the data in terms of distances from the absorber. Peak positions in this radial structure function roughly correspond to the radii of the scattering shells.[3]

Thus, atomic parameters such as N, R, and Z could be extracted directly from the EXAFS data. Before this time,

EXAFS data were compared with a theory function that used calculated values of these parameters. Because the values were often inaccurate, the data rarely correlated with theory. This lack of correlation had the net effect of calling into question the theoretical foundation of EXAFS. Introduction of the Fourier transform turned EXAFS into a viable experimental tool.

Since 1971, computer advances have allowed us to do away with many of the simplifying assumptions underlying the theory presented above. For example, Equation (7) assumes that the electron scatters as a plane wave from small, pointlike atoms. The effects of spherical wave scattering from more realistic atomic potentials can now be included. In addition, the scattering amplitude $f(k)$ can be replaced with an effective amplitude $f_{\text{eff}}(k,r)$ that has a weak radial dependence. This improvement to the theory has been incorporated into modern data analysis packages, such as the FEFF computer programs. (The name FEFF derives from f_{eff}.)

These programs also take multiple scattering into account, thus doing away with the single-scattering approximation. The effects of multiple scattering can sometimes make unexpectedly large contributions to the EXAFS. For example, in a face-centered cubic (fcc) solid such as δ-phase plutonium, the linear alignment of the absorber with atoms in the second and fourth shells creates a focusing effect that enhances the overall forward-scattering amplitude of the photoelectron by about a factor of 6 (at 0 kelvins). The phase shift is also enhanced, since a photoelectron is influenced by three or more atomic potentials as it journeys from the absorber to the second shell to the fourth shell and then back. The result is a "multiple-scattering" peak that overlaps with the location of the fourth shell. Analysis of the higher shells in the EXAFS would be difficult without the ability to handle these multiple-scattering peaks.

Extracting and Interpreting the Parameters. As outlined in Figure 6, the EXAFS is extracted from $\mu(E)$ based on an estimate of the free-atom absorption μ_0. The data are extrapolated to k-space, and amplitudes and phases can be either determined empirically or calculated. FEFF is used to fit $\chi(k)$ to a modern theory function through some variation of nonlinear least-squares curve fitting. Fitting the data before doing the Fourier transform avoids some issues of Fourier filtering (which can introduce errors into the data), but it is nonetheless difficult to evaluate the fit in k-space. Thus, as seen in Figure 6(c), both the data and the fit are transformed through a Fourier transform to a radial structure function. Inspection of the structure function provides the first insights into local structure. Information from other sources or from the EXAFS of a reference compound is then used to evaluate this initial model and to suggest ways to alter the fit criteria. These steps may be repeated numerous times, with the model being refined each time.

This iterative procedure is necessary because alone, EXAFS data is often too imprecise and the uncertainties in the fit parameters too large to support a definitive interpretation of the local structure. For example, the nominal uncertainty in determining the atomic number for each shell is $Z \pm 4$, and the uncertainty in the number of atoms in a shell can be as high as 30 percent. It is also impossible to calculate S_0^2 [see Equation (8)] to better than 20 percent. In addition, because all sites of an element contribute equally to the EXAFS, the data represent a population-weighted average of all the chemical species of an element that are present in the sample. The EXAFS cannot *a priori* distinguish between a sample containing one chemical species and another containing many species.

Furthermore, Equation (7) assumes that the radial positions of atoms in a shell are randomized according to a Gaussian distribution (through the parameter σ). Any non-Gaussian distribution, such as might result from a local strain or from the presence of different chemical species, is very difficult to handle analytically. An odd-shaped hump in the radial distribution function can be interpreted in terms of a chemical species that has several closely spaced shells, several chemical species coexisting in the same sample, or a sample that has a severe amount of disorder.

The imprecision can be partially resolved by simultaneously measuring the EXAFS from a reference sample. The reference is well characterized and will ideally contain only a single chemical species. We can then do a comparative analysis of the data and are limited only by the relative errors. Along those same lines, XAFS is best used to determine the differences between an unknown compound and a closely related, well-characterized compound, or to follow changes in a sample that is subjected to temperature, pressure, or chemical variations. With a well-planned set of experiments, XAFS is usually sufficient to detect changes in the local environment surrounding the central atom involving as few as one of its nearby neighbors.

Still, we often need to have a pretty good idea of what the local structure is before beginning an analysis. XAFS spectroscopy is therefore a tool that is most powerful when used in conjunction with other structure-determining methods, such as x-ray diffraction, Raman spectroscopy, or nuclear magnetic resonance spectroscopy. Ultimately, however, the ability to understand the local structure surrounding an element in an unknown environment depends on the skill of the experimenters and their analytical prowess.

[3]Peaks in the radial structure function do not correspond directly with shell positions. The phase shift $\Phi(k)$ in Equation (7) always contains a part that is linear in k—that is, $\Phi(k) = \phi k + \varepsilon(k)$, where ϕ is a constant and $\varepsilon(k)$ is a nonlinear function of k. The sine terms can therefore be written as $\sin((R+\phi)k + \varepsilon(k))$, and the Fourier transform of $\chi(k)$ actually produces a function $\chi(R+\phi)$. A detailed knowledge of the phase shift (either theoretical or empirical) is necessary to extract the shell radii. The radial structure function $\chi(R)$ is often plotted versus $(R-\phi)$ to emphasize this fact.

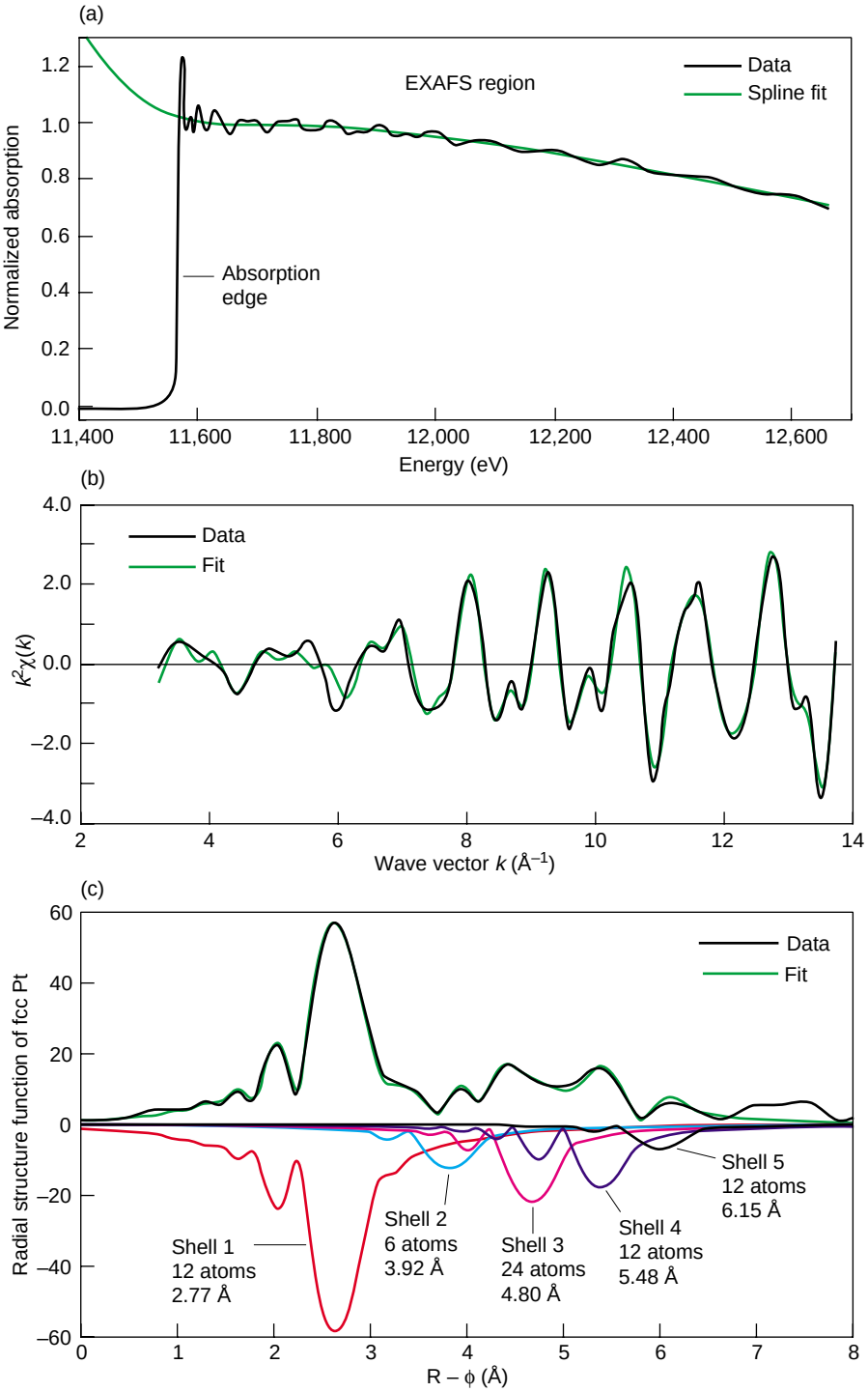

Figure 6. Analysis of a Platinum Foil

(a) The absorption coefficient $\mu(E)$ is obtained from the raw data (after correcting for the effects of various instrument defects or nonlinearities) by plotting $\ln(I/I_0)$ vs the x-ray energy, subtracting the background, and normalizing the edge jump to unity. The ionization potential energy E_0 is chosen, and the free-atom absorption coefficient μ_0 is approximated by a polynomial spline. (b) The EXAFS $\chi(k)$ is obtained by taking the difference between the data and the spline and converting the energy E to a wave vector k. As shown here, $\chi(k)$ is weighted by an arbitrary factor of k^2 to equalize the amplitude fluctuations at large k values and help avoid introducing errors in going from $\chi(k)$ to a radial structure function. Parameters are obtained by curve-fitting the data to a theory function such as Equation (7). (c) Taking the Fourier transform of $\chi(k)$ creates a radial structure function $\chi(R)$ that helps to illuminate shell positions. Platinum has an fcc crystal structure, and the positions of the first through fifth nearest-neighbor shells are at 2.772, 3.92, 4.801, 5.544, and 6.198 Å, respectively. The fit to $\chi(R)$ is shown by the green curve. Beneath $\chi(R)$ are the components of the fit that correspond to each shell. Note that the x-axis does not indicate radial distances in the structure that $\chi(R)$ represents. Because of the phase shift in the sine term in Equation (7), distances to nearby atoms are only approximated by peak positions in $\chi(R)$. The correct shell radii are obtained from the curve-fitting analysis.

Probing Chemical Speciation with XAFS

Chemical speciation (the individual compounds and complexes exhibited by an element that determine its reactivity) is particularly important in environmental science, because different compounds of a hazardous element can have greatly differing solubility and transport properties and differing effects on a biological system.

XAFS spectroscopy determines exactly those parameters needed to define chemical speciation: the valence of the central (absorbing) atom and the atom's radial structure function in terms of the atomic numbers of its neighbors, their distances from it, and the number of each type of atom at each distance. In addition, the elemental specificity of XAFS precludes interference from other compounds. This means that little or no sample preparation is required, and thus there is no need for a separations process that could inadvertently alter the speciation. Even intensely radioac-

tive sludge from a Hanford waste-storage tank (containing dozens of elements in a dense, complicated matrix) relinquishes speciation information on its elements when small samples are placed in the XAFS beam.

Speciation of Uranium in Soils. During the Cold War, the Feed Materials Production Center in Fernald, Ohio, was a DOE plant that processed uranium. When the plant closed after nearly 40 years of operation, some of the soil around it was contaminated with up to several thousand parts per million of uranium. A number of DOE-sponsored research and development projects were begun to develop a cost-effective method for washing the uranium out of the soil.

Even if accurate records of individual spills had been maintained, decades of weathering had ensured that the uranium species in the soil were substantially altered from their original forms. Various techniques, including ultraviolet-induced fluorescence and electron microscopy, showed that the uranium was present as discrete particles adhering to the soil's mineral grains. Those detection methods, however, could not identify the exact uranium species, and the efficiency of proposed extraction methods depended on such information. Thus, XAFS was selected as one of the primary characterization techniques. This marked its first use as a routine analytical tool for a project of this magnitude.

XAFS quickly proved itself. Even with the most rudimentary sample preparations—simply removing pebbles and grass stems and then lightly grinding the remaining soil with a mortar and pestle—XANES spectra revealed the presence of the characteristic "-yl" shoulder of the uranyl O=U=O unit. (Refer to the XANES box on page 432.) Although XAFS probes all uranium species simultaneously, observation of this feature in all samples demonstrated that the soils contained a significant fraction of standard U(VI) species. At four site locations, the fraction of U(VI) was greater than 80 percent.

Analysis of the EXAFS confirmed that initial identification, for it found a U–O distance corresponding to the uranyl bond length of about 1.74 angstroms. It also found other U–O distances between 2.3 and 2.4 angstroms that are typical of oxygen-containing ligands such as O^{2-} or OR^{-} (where R is a chemical group) that bond in the equatorial plane of U(VI) complexes. The remainder of the uranium in the soil appeared to be a non-UO_2 species of U(IV).

Our finding that the uranium existed mostly as U(VI) species was important. It immediately eliminated from consideration proposed separation methods targeted at the chemical or physical properties of U(IV), which had been promoted as the most stable oxidation state of uranium under site conditions.

Elucidating the particular species of U(VI) or U(IV) proved to be difficult, however. For the most part, identifiable features could be culled from the data for only the first shell of neighboring atoms, which were nearly always oxygen. But the analysis was too uncertain to indicate specifically which ligands were present. One interesting conclusion could be drawn, however. Because samples were taken from different soil layers, we could observe the evolution (by equating soil depth with time) of chemical structures. The solids seemed to become more crystalline with age.

Following this initial characterization, XAFS was used to help develop soil-washing methods. We tested one method that used citrate as a complexing agent (a method commonly used in mining). We also explored a more selective soil-washing method that used Tiron as a complexant in conjunction with a mobilizer, dithionite. The washing methods readily removed the bulk of the uranium but left behind an intractable fraction. In the XAFS spectra, soil washing reduced the "-yl" shoulder in the XANES and reduced the amplitude of the actinyl contribution in the EXAFS. Taken together, those two changes indicated a selective loss of U(VI) and an increase in the U(IV):U(VI) ratio.

To quantify this effect, we first needed to devise a method to analyze the XANES. For this series of experiments, performed around 1990, we could not use the energy of the absorption edge to identify the oxidation state of the species in the sample because we could not obtain a reliable edge energy. During the course of an experiment, the drifts in the monochromator and the beam location are irreproducible. Typically, the spectrum of a thin metal foil is taken simultaneously with one of the sample, and the known characteristics of the foil spectrum are used to correct for instrument drifts. However, uranium metal could not be used as a calibration standard because it oxidizes too rapidly when exposed to air, even when protected by a film of acrylic resin. Furthermore, we could not use UO_2 or some other reference oxide for this calibration since it would suffer from a change in the incident beam intensity when the uranium oxide in the sample absorbed the x-rays. Finally, the absorption edge of another, more stable element was too far away to be a good calibration standard.

The problem of getting a reliable edge energy was solved by always assigning the inflection point in the absorption edge to the same energy. The edge was then fit with a particular combination of Gaussians and an arctangent. This method had the advantage that the position of the Gaussian corresponding to the "-yl" shoulder could be found with high accuracy even in relatively noisy data. The difference in energy between the U(VI) absorption edge and the shoulder is relatively invariant since the former depends largely on the ionization potential energy of the U(VI) species and the latter on the U=O bond length in the actinyl moiety, which does not change between different U(VI) complexes. As the percentage of U(IV) increased, the energy of the sample's absorption edge decreased since it is the average of the U(IV) and U(VI) edge energies. Hence the energy difference between the inflection point and the Gaussian increased, and this

XANES

The x-ray absorption near-edge structure (XANES) refers to the secondary peaks and shoulders that modify the appearance of the absorption edge and the 20- to 30-eV region beyond it. The XANES can reveal the oxidation state of an element in the sample, as well as serve as a "fingerprint" to identify certain structural motifs of a chemical species.

The energy at which an absorption edge appears depends on the ionization potential E_0 of the absorbing atom, but in general E_0 increases when the absorber is in a higher oxidation state. The accompanying figure shows XANES spectra of the Pu(III) and Pu(VI) aquo ions, $Pu(H_2O)_n^{3+}$ and $PuO_2(H_2O)_m^{2+}$, respectively. The absorption edge shifts toward higher energies with higher oxidation states. After gathering XANES data from several oxidation-state-pure samples, we can construct a curve of oxidation state versus edge energy. This calibration curve can then be used to identify the oxidation state of the various plutonium species in unknown samples.

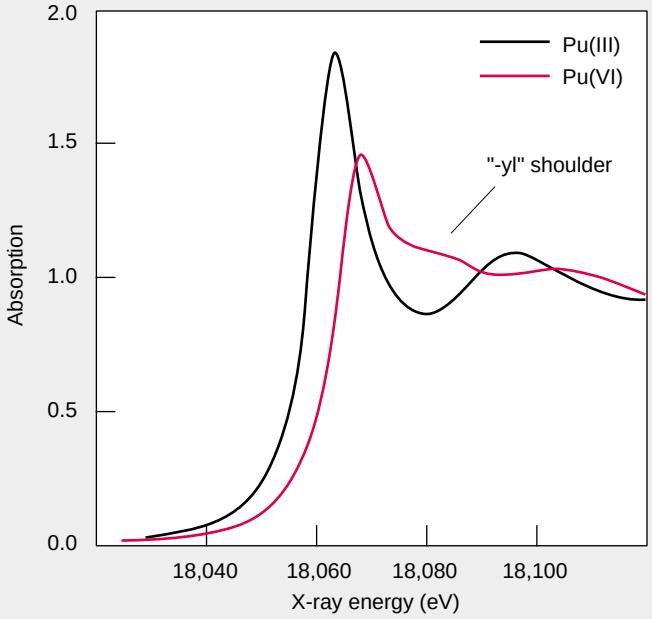

The presence of certain molecular structures can also be inferred from features in the XANES. For example, in an aqueous solution, uranium, neptunium, and plutonium ions in the V and VI oxidation states nearly always exist as actinyl ions. The actinyl is a *trans*dioxo cation with a linear structure: two oxygen atoms form strong, covalent bonds to the central actinide, O=An=O, where An can be uranium, neptunium, plutonium, or americium. The actinyl generates a distinctive "-yl" shoulder in the XANES at energies just above the absorption edge. The presence of this shoulder can be used to confirm the presence of the An(V) or An(VI) oxidation state in complex chemical matrices.

difference was used to track the U(IV):U(VI) ratio. We were able to confirm the presence of an easily removed U(VI) fraction and a much more inert U(IV) compound that was not UO_2 (see Figure 7).

Over two and a half years, we obtained and analyzed spectra from almost 60 samples, demonstrating the feasibility of using XAFS as a routine, albeit complicated and high-powered, analytical tool for determining average chemical speciation in complex environmental samples. Although our XAFS information could have been used to optimize cleanup operations, ultimately none of the soil-washing methods was used at Fernald. Because of the anticipated cost of all proposed schemes, the immediate problem was solved by loading the more heavily contaminated soils into drums and trucking them to a chemical waste dump for indefinite storage.

Pu(IV) Colloid. In many natural water systems, such as aquifers or oceans, plutonium is in the IV oxidation state. However, measurements of the total Pu(IV) concentrations in synthetic waters that mimic natural conditions vary wildly—by many orders of magnitude. The huge variations are likely due to the presence of Pu(IV) oxyhydroxide, more commonly known as Pu(IV) colloid.

Colloids consist of tiny, 1- to 1000-nanometer-sized particles that remain suspended in solution. Laboratory-based x-ray diffraction patterns of aged Pu(IV) colloids display Bragg peaks that are similar to the fcc structure of plutonium oxide, PuO_2. This similarity led to the assumption that the colloids are tiny crystallites of plutonium oxide, perhaps with a water-saturated, or hydrated, surface. But our XAFS studies of Pu(IV) colliods demonstrated that this average fcc structure is overly simplistic and that additional chemical moieties are present that could substantially affect the colloids' solubility. Thus the variations in measured Pu(IV) concentrations may in fact be related to the local structure of the colloid particles.

Instead of the displaying the single Pu–O distance of the oxide (2.34 angstroms), the colloid displays many discrete Pu–O distances that are easily and unequivocally identified, ranging from 2.25 angstroms—characteristic of Pu–OH moieties—up to about 3.5 angstroms (see Figure 8). Also, relative

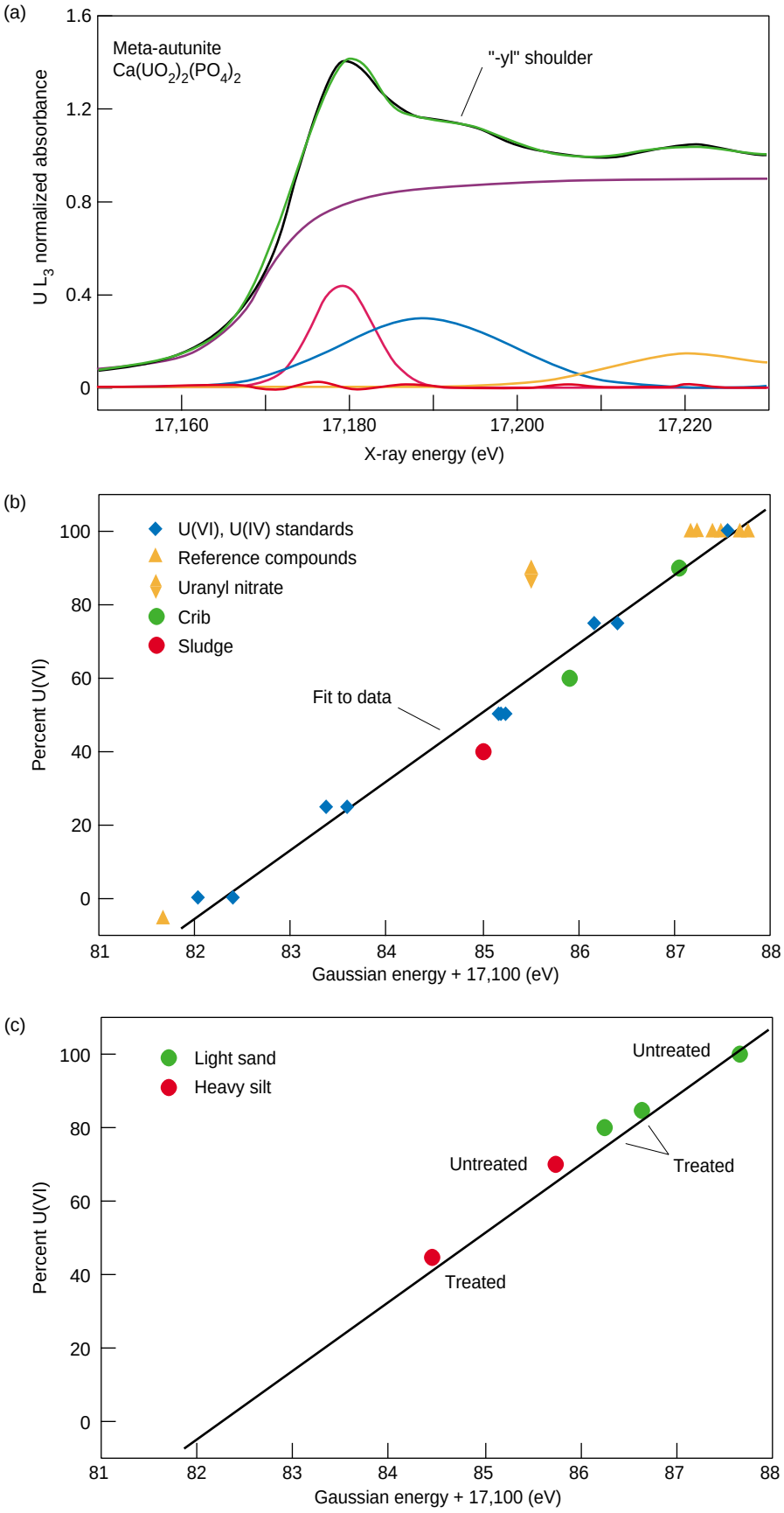

Figure 7. Determination of the U(IV):U(VI) Ratio for Washed Fernald Soils

(a) We used XANES spectra to identify the oxidation state of uranium complexes in soils around the Fernald plant. The XANES data were fit with a combination of Gaussian functions and an arctangent. The "-yl" shoulder at energies just above the main peak is indicative of U(VI). The position of the Gaussian corresponding to this feature could be found with high accuracy and could be used to track the U(IV):U(VI) ratio. (b) We used various mixtures of UO_2, a U(IV) species, and meta-autunite, a U(VI) species, to obtain a ratio-vs-energy calibration line. Significant uncertainties were observed only at the lowest U(VI) concentrations, when the intensity of the "-yl" shoulder was very small. We deduced that our technique was accurate to within ±10% when tested with a number of standards possessing a range of local structures. Soil (crib) and tank-sludge samples taken from the Hanford site also fell reasonably close to the curve. (c) Many of the Fernald soils had high quantities of U(VI) species, although there was a significant variation between samples. The application of our Gaussian technique to the analysis of washed Fernald soils showed that, in general, washing removed U(VI) but left the less soluble U(IV) in the soil.

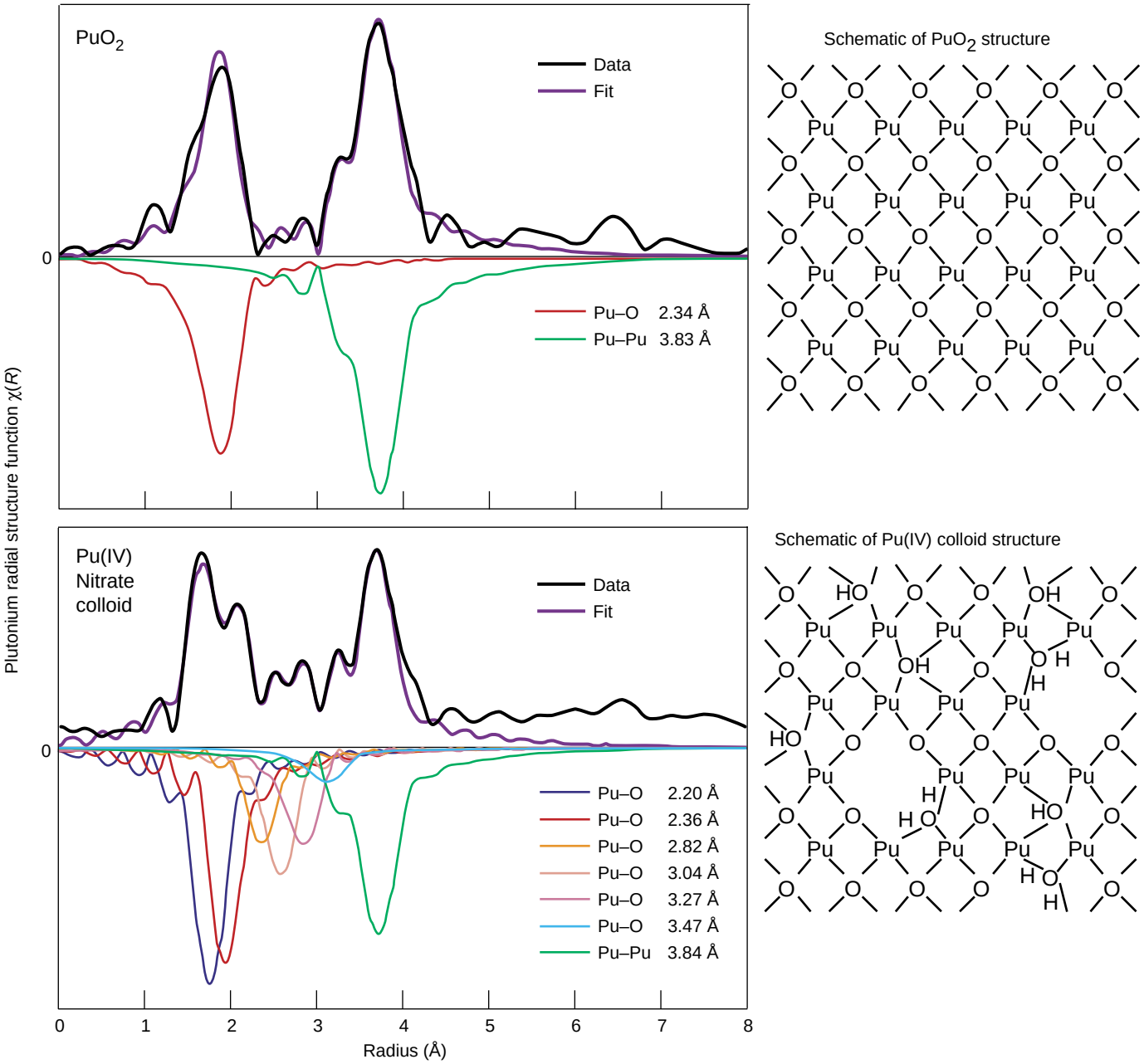

Figure 8. Plutonium(IV) Colloid

The Fourier transform for the EXAFS of PuO_2 (lower figure) shows some deviations from a highly ordered fcc crystal structure, but no shells other than the Pu–Pu and Pu–O. The Pu–Pu peak has a relatively large amplitude. The EXAFS of the Pu(IV) colloid (top figure) shows a reduced Pu–Pu amplitude and a plethora of Pu–O distances, including the one native to PuO_2. The Pu–O distance of 2.20 Å is indicative of a hydroxide ligand. These results suggest a model for the colloid: every four protons incorporated into the structure produce a plutonium vacancy. The different types of oxygen ligands will form different types of bonds with the plutonium, resulting in the series of well-defined bond lengths observed in the EXAFS. We expect that the plutonium atoms will also undergo displacements but that the average long-range order will be conserved. Portions of the material with plutonium vacancies, hydroxides, and water concentrations could be expected to form unique domains, as indicated in the two-dimensional diagram on the right. Different domains may have different structures and properties.

to the oxide's EXAFS, the amplitude of the Pu–Pu peak in the colloid's EXAFS is considerably reduced. By a simple charge-balancing argument, four hydrogen atoms incorporated into the Pu(IV) colloid structure could result in one plutonium-ion vacancy. Thus the reduced amplitude may indicate an actual decrease in the average number of plutonium nearest neighbors.

The fact that the Pu(IV) colloid displays a diffraction pattern tells us that the plutonium sublattice of the PuO_2 crystallite is retained on average. However, the EXAFS reveals that many atoms in the colloid structure are distributed in a non-Gaussian way when compared with their placement in the Pu(IV) oxide. This distribution again suggests that several different oxygen-containing groups are present in the colloid. In addition to the original O^{2-}, there may be OH^- and possibly OH_2. This variety would further imply that the Pu–Pu distance distribution would have to display concerted excursions from the average unit cell.

Defects in the average structure of the Pu(IV) colloid could create chemically distinct domains within the colloid particle. If the Pu(IV) colloid has domains that are more properly described by, for example, $Pu_5O_8(OH)_4$, then the colloid's behavior in a natural system would be altered in comparison with a suspension of PuO_2 crystallites. Depending on the specific domain structure, the colloid could even exhibit a range of solubilities, and its behavior in a natural waters could be quite variable. By extension, defects in the local structure of other plutonium precipitates could to a large degree determine the behavior of those plutonium complexes in the environment.

Summary

Although not yet mature in the sense of being a routine spectroscopy, XAFS is already contributing to our understanding of environmental science and the nature of atomic structure in solids. Its contribution will only increase as the field expands and the technique becomes standardized. Furthermore, the increased brightness of the next-generation light sources should enable x-ray beams of submicrometer dimensions within the next few years. Such a source will allow us to identify individual domains within a target sample, with significant applications to geochemistry, materials science, and bioremediation.

As discussed in numerous articles within this volume, our XAFS studies have helped us deduce the basic structure of plutonium complexes in matrices that are relevant to many areas of plutonium science. For example, our studies of plutonium in carbonate solutions have contributed to a basic understanding of the long-term viability of a nuclear-waste repository at Yucca Mountain, where carbonate waters abound. We have also studied actinide species in Hanford waste tanks and in the vitrified glass logs that are being considered for storage within Yucca Mountain. Our XAFS studies of plutonium in nitric acid solutions are important for improving our plutonium waste-treatment processes, and our investigations into the local structure of δ-phase plutonium have provided some insight into the aging of weapons-grade plutonium and the behavior of complex materials. We expect that our XAFS work will also contribute to a broader, more fundamental understanding of plutonium and the other actinides. ■

Further Reading

Conradson, S. D. 1998. *Applied Spectroscopy* **52**: 252A.

Stern, E. A. 1988. Theory of EXAFS. In *X-Ray Absorption: Principles, Applications, Techniques of EXAFS, SEXAFS and XANES.* New York: John Wiley and Sons.

Steven Conradson obtained his B.S. in chemistry from San Jose State University and his Ph.D. in physical chemistry from Stanford University, where he used XAFS spectroscopy to determine structural information about the molybdenum site in nitrogenase. He spent two years at Harvard University on a National Institutes of Heath postdoctoral fellowship, performing XAFS and nuclear magnetic resonance measurements on the nitrogenase iron-molybdenum cofactor. Coming to Los Alamos as a postdoctoral fellow, he was subsequently hired as a technical staff member and is now the XAFS project leader in the Structure/Property Relations Group of the Materials Science & Technology Division. He initiated the ongoing program at the Stanford Synchrotron Radiation Laboratory for applying synchrotron x-ray methods to determine local structure and chemical speciation in radioactive samples. In collaboration with various national laboratory and university groups, he has participated in many projects involving environmental, separations, and fundamental actinide chemistry. His recent interests involve investigating nanoscale heterogeneity in both amorphous and crystalline systems as the origin of complex behavior.